Impact of Weather Systems on UAV Parameters Using Computational Fluid Dynamics

Saif Aljuhaishi

Yaseen K. Al-Timimi

Basim I. Wahab

Impact of Weather Systems on UAV Parameters Using Computational Fluid Dynamics

Abstract

Since drones cannot fly in any kind of weather, they are not safe for time-sensitive activities. The study examines how the passage of weather systems in Iraq leads to the ban on drone flights, and how these weather conditions impact the aerodynamic forces of the drone. Hourly climate data for the study area were obtained from ECMWF ERA5 and CAMS in NetCDF format for four climate stations (Erbil, Baghdad, Rutbah, and Basrah). A ScanEagle drone was chosen for this study. The Python programming language was used to perform mathematical operations to calculate the ban on drone flights. ArcGIS 10.8 was used to create maps of the spatial distribution of the Python results. 80 ScanEagle flight scenarios were investigated in a wind tunnel simulation using computational fluid dynamics. Ansys 2019 was used to perform the simulation. The results showed that Red Sea and mid-latitude depressions had the most effects on drone flight in Iraq because they increased aerodynamic forces (lift and drag), which in turn increased the power needed for constant speed flight. This resulted in an increase in fuel consumption and flight duration. Red Sea depressions mostly affect the center and southern parts of Iraq; on the other hand, mid-latitude depressions mostly affect the northern and western regions, and when flying at 700 hPa, they affect the entire country.

Keywords

ScanEagle, UAV, python, CFD, Ansys, ArcGIS.

RESEARCH PAPER

Impact of Weather Systems on UAV Parameters Using Computational Fluid Dynamics

Saif Aljuhaishi*, Yaseen K. Al-Timimi, Basim I. Wahab

Department of Atmospheric Sciences, College of Science, Mustansiriyah University, Baghdad, Iraq

Abstract

Since drones cannot fly in any kind of weather, they are not safe for time-sensitive activities. The study examines how the passage of weather systems in Iraq leads to the ban on drone flights, and how these weather conditions impact the aerodynamic forces of the drone. Hourly climate data for the study area were obtained from ECMWF ERA5 and CAMS in NetCDF format for four climate stations (Erbil, Baghdad, Rutbah, and Basrah). A ScanEagle drone was chosen for this study. The Python programming language was used to perform mathematical operations to calculate the ban on drone flights. ArcGIS 10.8 was used to create maps of the spatial distribution of the Python results. 80 ScanEagle flight scenarios were investigated in a wind tunnel simulation using computational fluid dynamics. Ansys 2019 was used to perform the simulation. The results showed that Red Sea and mid-latitude depressions had the most effects on drone flight in Iraq because they increased aerodynamic forces (lift and drag), which in turn increased the power needed for constant speed flight. This resulted in an increase in fuel consumption and flight duration. Red Sea depressions mostly affect the center and southern parts of Iraq; on the other hand, mid-latitude depressions mostly affect the northern and western regions, and when flying at 700 hPa, they affect the entire country.

Keywords: ScanEagle, UAV, Python, CFD, Ansys, ArcGIS

1. Introduction

Unmanned Aerial Vehicles (UAVs) are a new technology that has recently transformed the commercial, military, and civilian domains [1]. UAVs are typically chosen for missions that require a lot of pilot effort and that are deemed hazardous. They can be used for a variety of tasks, such as road traffic, search and rescue operations, border patrol missions, and fire monitoring [2,3]. Although UAV systems come in a variety of sizes, from small to very large, there are meteorological conditions that restrict or eliminate their use [4]. The advent of UAVs has brought forth a number of challenges, including making sure they operate safely throughout missions. UAV safety is a delicate and uncharted area because unexpected drone behavior or dangers present a significant risk [5,6].

In Iraq, weather systems affect the temperature, precipitation patterns, and climate of the several seasons [7]. The amount of rainfall in the area is influenced by pressure systems, particularly those that move over the nation in the spring, autumn, and winter rainy season [8]. From June to September, Iraq encounters hot and arid weather conditions during the summer months [9].

1.1. Literature

Reference [10] present a data-driven method for assessing the risks connected to drone operations in urban airspace by examining meteorological data from 63 locations in Singapore. It finds notable trends in annual meteorological data and classifies risk levels based on geographic region. This enables the development of an environmental risk map for the purpose of planning safe drone operations. Reference [11] provided a system that integrates qualitative and quantitative techniques to ensure drone safety over the Internet of Drones (IoD). For

Received 9 September 2024; revised 21 October 2024; accepted 25 October 2024.
Available online 29 November 2024

* Corresponding author.
E-mail address: saifaljuhaishi@uomustansiriyah.edu.iq (S. Aljuhaishi).

https://doi.org/10.33640/2405-609X.3381

hazard identification, risk assessment, and mitigation, the qualitative approach adheres to International Organization for Standardization (ISO) 12100 and ISO 13849 requirements, whereas the quantitative strategy uses Bayesian networks for probabilistic modeling of safety problems. Stakeholders can address UAV safety issues by using a case study of a UAV crash to demonstrate the applicability of both approaches. Reference [12] provided an overview of the weather observation and avoidance systems needed to support the developing drone economy was provided by. Reference [13] used computational fluid dynamics to investigate the effects of downtown Toronto buildings on wind fields, a crucial component of drone operations. By dividing the city into 20 zones and combining historical meteorological data with Computational Fluid Dynamics (CFD) derived wind velocities, it produces an RMSE of 8% for bearings and 12% for wind velocities, respectively. The results facilitate the development of historical, real-time, and predicted wind field representations, hence increasing drone flying safety and efficiency. Reference [14] researches UAV risk assessment. The Expected Level of Safety (ELS) analysis is a crucial part of safety issues. Two case studies of Unmanned Aircraft Systems (UAS) logistic delivery are tested in order to validate the UAS services. The case studies offer enough information to enable UAS logistic delivery in Taiwan's remote and suburban areas with suitable path planning, enabling an analysis of the ELS to ground risk and air risk. Reference [15] introduced A tool for probabilistic risk assessment of fixed-wing UAV missions called DROSERA. It calculates the likelihood of accidents or casualties due to UAV loss of control. It integrates several models, including the most recent versions of models for risk mitigation strategies, time of day sensitivity, and wind effects. In order to illustrate the synthesis, required inputs, and outputs of the tool, a semi-urban UAV mission is used. Reference [16] examine and enhance UAV capabilities with an emphasis on analysis, In order to boost productivity and safety during routine flights. When determining hazard, it considers important variables such as battery condition, temperature, and power consumption for energy-efficient UAVs. The technology assesses danger both before departure and during the flight using actual flight conditions and provided battery statistics. Reference [17] investigated and improved the functional properties of UAV, with an emphasis on analysis to increase efficiency and safety for routine flights. Important factors, including battery state, temperature, and power usage for energy-efficient UAVs, are taken into account when calculating hazards. The technology uses real flying conditions and battery statistics to evaluate danger before takeoff and during the flight. Reference [18] looked at extreme weather conditions that affected civil aviation flights at Iraqi airports, they found that dust storms had the most effect on the airports in Najaf and Basra, while fog had the greatest effect on Baghdad International Airport. Thrusters and snow also had a major effect on the airports in Erbil and Sulaymaniyah.

Nomenclature

UAVs	Unmanned Aerial Vehicles
IoD	Internet of Drones
ISO	International Organization for Standardization
CFD	Computational Fluid Dynamics
ELS	Expected Level of Safety
UAS	Unmanned Aircraft Systems
PSL	Physical Sciences Laboratory
NetCDF	Network Common Data Form
ECMWF	European Centre for Medium-Range Weather Forecasts
ERA5	ECMWF Reanalysis v5
CAMS	Copernicus Atmosphere Monitoring Service
ISR	Intelligence, Surveillance, and Reconnaissance
T	Temperature
PRE	Pressure
Visib	Visibility
RANS	Reynolds-veraged Navier−Stokes equations
PR	Power Required

Due to the lack of studies examining the impact of weather conditions on drone flights in the Middle East, especially in Iraq, most studies focus on the use of civilian drones in urban environments and in areas far from the study area. This study investigates the effect of weather conditions associated with weather systems on the aerodynamic forces of drones in Iraq. This was done by examining 80 drone flight scenarios in a wind tunnel experiment using computational fluid dynamics in Ansys 2019. Python programming language was also used to calculate the number of flights ban hours for ScanEagle in Iraq in the presence of weather systems. ArcGIS v.10.8 was used to create spatial distribution maps of the Python results.

2. Materials and methods

2.1. Study area

Iraq is located in the northern hemisphere of the earth, between 29° 05 and 37° 23 north and 38° 45 and 48° 45 south. Its borders are as follows: Saudi Arabia, Syria, and Jordan border it on the west; Kuwait and Saudi Arabia border it on the south; Iran borders it on the east [19,20]. Iraq spans a total area of 438,320 km^2. There are mountains around to the north, northeast, and east; some of them are as high as 3607 m above Sea level. A sedimentary plain separates the plateau that makes up eastern Iraq from the mountains [21]. The research area is depicted in Fig. 1. Iraq's continental climate is characterized by hot, dry summers and mild, rainy winters with a predominance of northwesterly winds. Storms that sweep eastward and across northern Iraq are mostly responsible for the winter rainfall in the Mediterranean region [22,23]. Winters are often cool to cold, with daily highs as high as 16 °C and lows of 2 °C at night. The summers are hot and dry, with highs of around 43 °C in July and August and lows of about 26 °C at night [24]. Rainfall in Iraq is classified as seasonal; in the north and northeast, the country's rainy season lasts from November to April. The winter months of December through February bring rain to the remainder of the nation. The Zagros and Taurus mountains of Iraqi Kurdistan are located in the northeastern part of the country, which receives 700−1000 mm of precipitation annually. The rest of the country, which is composed of plains and hills, is arid. The annual rainfall in the lowlands ranges from 100 to 180 mm [25,26]. There is 192.03 mm of precipitation on average every year [27]. Two different wind patterns are responsible for the dust storms that occur in Iraq during the spring season: the Al-Khamsian wind and the North wind, which has historically caused dust storms in this region [28].

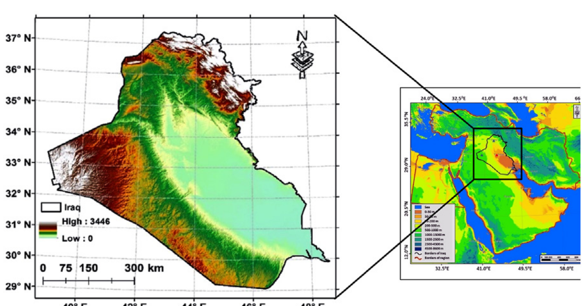

Fig. 1. Study area.

2.2. Data

Using daily synoptic map analysis from the NOAA Physical Sciences Laboratory (PSL) website [29], case studies of weather systems were chosen. PSL is a specialized research facility devoted to meteorological and physical oceanographic research in various fields. Researchers at PSL work on a range of topics, including atmospheric variables, oceanic gravimetry, internal wave dynamics, and acoustic noise fields [30]. Synoptic maps of the weather systems chosen for this research are shown in Fig. 2. Choosing the level (1000) and observations (1200) millibars for each of the four study stations. Table 1 includes the selected cases.

Temperature, precipitation, relative humidity, and wind speed data were collected in Network Common Data Form (NetCDF) format from the European Centre for Medium-Range Weather Forecasts

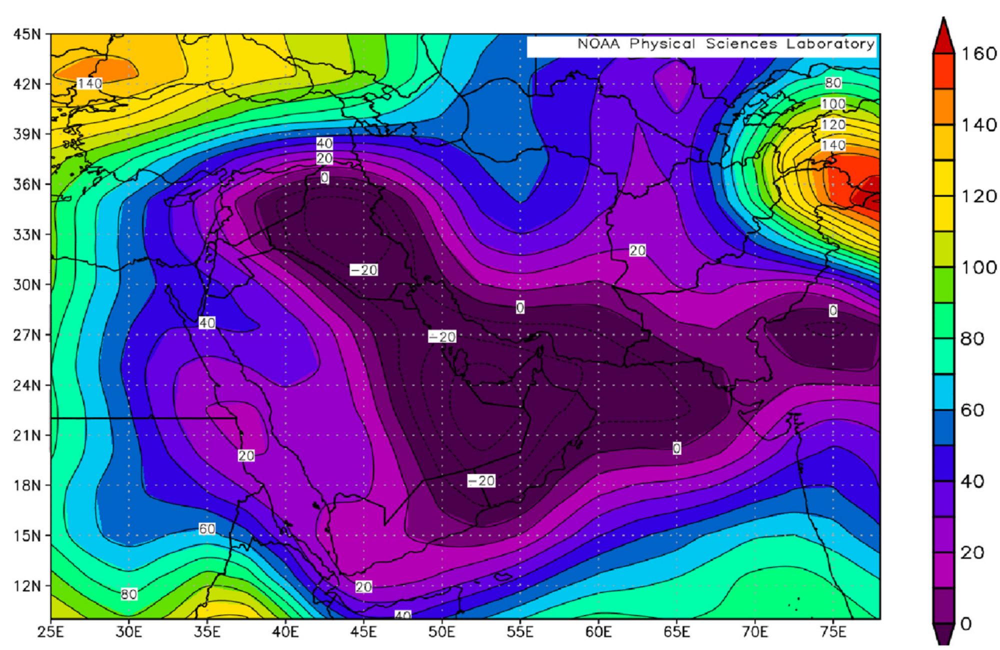

Fig. 2. The geopotential height synoptic map for Middle East on July 24, 2023.

Table 1. Case studies of weather systems.

Weather systems	Date
Mid latitude depression	7 February 2023
Red Sea depression	26 March 2023
Subtropical high	14 April 2023
Monsoon low	24 July 2023
Siberian high	27 December 2023

(ECMWF) Reanalysis v5 (ERA5) [31], the fifth generation ECMWF reanalysis of the world's weather and climate over the previous eight decades [32], for use in case studies of pressure systems in Iraq and as inputs for simulation scenarios. ECMWF the Copernicus Atmosphere Monitoring Service (CAMS) used to acquire visibility data. When analyzing the atmosphere, the CAMS focuses on the chemical species, aerosols, and greenhouse gases that make up the atmosphere [33]. When examining chemical species and aerosol concentrations, CAMS fits more accurately than conventional meteorological fields [34]. For the ERA5 data and the CAMS data, the cell size was 0.25 and 0.4, respectively. Every single byte of information was in NetCDF format, using a 20-bit.

2.3. Drones and weather conditions limitations

We should take into account the constraints of the weather when launching and flying the drone, as failure to do so may result in damage or even loss. Depending on the kind of aircraft and how it was made, this restriction changes. ScanEagle, shown in Fig. 3, was selected in this study. The US military has been using Insitu, a Boeing Company's adaptable Intelligence, Surveillance, and Reconnaissance (ISR) unmanned aerial vehicle platform, ScanEagle, both on land and in the water, since 2004. ScanEagle has been used globally by governmental, military, and commercial organizations [35]. These relatively simple systems offered the benefit of being easy to use, integrate, maintain, and repair, which made them ideal at the tactical level. They may also swiftly change the payloads they carried [36]. The aircraft is a good fit for the synoptic overview duty due to its unique performance characteristics and sensor specifications that make it stand out when used in large-scale fires [37]. Numerous studies on the use of UAVs for wildlife monitoring have made use of ScanEagle [e.g., [38,39]]. The company's Australian affiliate, Insitu Pacific Pty Ltd, installed a stills camera payload onto its ScanEagle UAV and operated the system for this testing [40]. Table 2 show ScanEagle technical specifications and weather conditions limitations.

Fig. 3. ScanEagle drone [35].

2.4. Methodology

The scientific content of the study can be discussed under two headings:

In the first part, the previously determined launch and flight limitations of the selected UAV (ScanEagle) were compared with the regional and time-dependent effects of whether the dominance of 5 weather systems was effective in Iraq. Then, the frequency of times not suitable in terms of launching and flight across the country is determined for each weather system.

In the second part, based on atmospheric data both at ground level and at 700 hPa, for a total of 80 scenarios (5 weather systems * 4 stations* at 2 different times of the day), the lift and drag forces on the UAV and power required for it to cruise at 25 m/s speed have been calculated. These calculations are based on the geometry of a defined air tunnel.

In the first part of the research, the climate data for the two levels the surface level affects the launch of the drone, and the 700 hPa level affects the flight of the drone at this level were compared with the selected cases of weather systems with weather limitations for ScanEagle. Through which the percentage frequency of flying ban caused by weather hazards for launching and flying the drone was calculated. Visibility <500 m, which restricts operators from launching drones at surface level, which

Table 2. ScanEagle technical specifications and weather limitations [41].

Feature	Value
Wingspan (m)	3.1
Weight (kg)	22
Max speed (m/s)	40
Max altitude (m)	5000
Endurance (h)	12
Wind (m/s)	18
T_Min (ºK)	263.15
T_Max (ºK)	323.15
Precipitation (mm)	>0

arises due to fog and dust storms. At 700 hPa level relative humidity >90% may represent areas of cloud formation or thunderstorm areas, and low visibility may restrict flying at high levels and affect the operation of the drone's electronic circuits as well as the internal combustion process in the engines. The data on climate was analyzed using the Python programming language. After comparing the hourly climate data for the research area with weather restrictions for drone flights, the NetCDF files were transformed into zero matrices for the climate component. The frequency with which weather-related drone flight prohibitions occurred was then tallied hourly and for each pixel in the study region (see Fig. 4). Every component of the climate underwent the same set of procedures. Finally, it generates a NetCDF file with a single-layer matrix that shows, for each pixel during the study period, the percentage of flight ban frequency caused by weather hazards. With ArcGIS 10.8, the Make Raster from NetCDF tool in the Multidimension toolbox was used to convert NetCDF, which was the output of Python data processing, to a raster. The frequencies that blocked flight due to weather hazards were totaled for each pixel in the rasters for the elements that resulted from the first stage using the Cell Statistics tool in the Raster Analysis toolbox. The contour tool was used to draw contour lines. Using a single, predetermined legend, the maps were classified for the dangers of each element over the study area. At last, the maps were finalized in terms of layout, and further elements were added. The study technique flow chart was displayed in Fig. 5.

In the second part, Computational Fluid Dynamics (CFD) was used through Ansys 2019 software to simulate the wind tunnel experiment of flying a ScanEagle drone, using 80 scenarios for the weather conditions accompanying the weather systems at four points representing weather stations distributed over the area of Iraq. Then the average of the simulation results was calculated at the Iraq level. The aerodynamic parameters, lift and drag forces, of the drone were calculated and compared. The power required to fly the ScanEagle under the same conditions was then calculated for the weather systems. Fig. 6 presents the methodology for the second part of the research. ANSYS 2019 programs were used to modify and process the drone design. The Reynolds-Stress Transport model was chosen as the most accurate to simulate the wind tunnel experience for the scenarios. SpaceClaim and DesignModeler 2019 were used to modify the drone model and create domains. ANSYS mesher were used to generate the mesh. Ansys fluent was used to set up the CFD simulation, prepare general assumptions, determine the turbulence and dispersion models, and prepare boundary conditions for the wind tunnel experiment. Ansys solution was used to set the solution parameters, controls, and methods. Before importing in ANSYS Fluent 2019, it was necessary to design the geometry in AutoCAD software and perform further operations in SpaceClaim and DesignModeler. Table 3 shows the scenarios and inputs for the wind tunnel experiment in the surface layer, and Table 4 shows the scenarios and inputs for the wind tunnel experiment at the 700 hPa level.

```python
# Define the boundary conditions for each variable
boundary_conditions = {
    'tmax': {'var': 't2m', 'condition': lambda x: x >= 323},
    'tmin': {'var': 't2m', 'condition': lambda x: x <= 263},
    'pre': {'var': 't2m', 'condition': lambda x: x > 0},
    'wind': {'var': 'wind_speed', 'condition': lambda x: x >= 15},
    'visibility': {'var': 't2m', 'condition': lambda x: x < 500},
}

def apply_conditional_limits(ds, boundary_conditions):
    result_ds = xr.Dataset()
    for key, cond in boundary_conditions.items():
        var = cond['var']
        condition = cond['condition']
        data_array = ds[var]
        conditioned_array = xr.where(condition(data_array), 1, 0)
        result_ds[key] = conditioned_array
    return result_ds

# Apply conditional limits
conditioned_ds = apply_conditional_limits(ds, boundary_conditions)
```

Fig. 4. The program written in Python.

The wind speed at zero angle of attack of the drone was assumed based on the drone's boundary conditions from the manufacturer and also the highest wind speed the drone can withstand.

The coupled method was used to solve the Reynolds-averaged Navier−Stokes equations (RANS), continuity equation, and energy equation, which represent conservation of momentum, conservation of mass, and conservation of energy, respectively. As well as to solve the three-dimensional equations of turbulent kinetic energy. In the aforementioned equations and the turbulence model equations, residual monitors were 10-6. The solution will keep solving until it reaches convergence or finishes 100 iterations.

The Mach number (0.11655) has negligible compression effects that can be disregarded at Mach values lower than 0.3. As a result, assumptions included steady state, absolute velocity, and incompressible stream. It is assumed that the flow is adiabatic, meaning that there is no heat exchange between the ambient air and the drone. The gravitational acceleration with respect to Earth is 9.8 m/s^2. In order to replicate the region where the wind tunnel experiment will be conducted, two 3D domains have been constructed around the drone

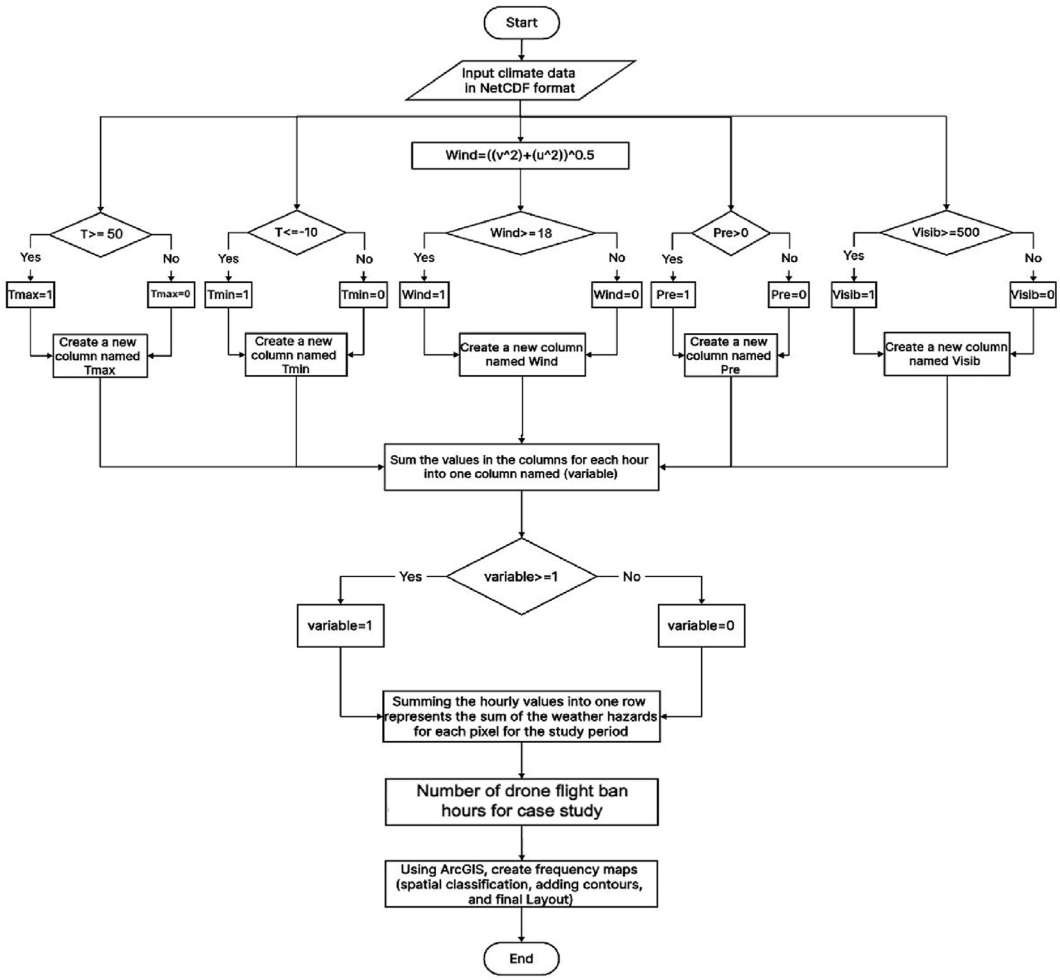

Fig. 5. The research methodology.

model, adhering to best practice principles. In Fig. 7, its dimensions are displayed. As can be seen in Table 5 and Fig. 8, both domains were meshing with distinct features for each other. In total, there were 15,823,231, and 3,112,852 nodes.

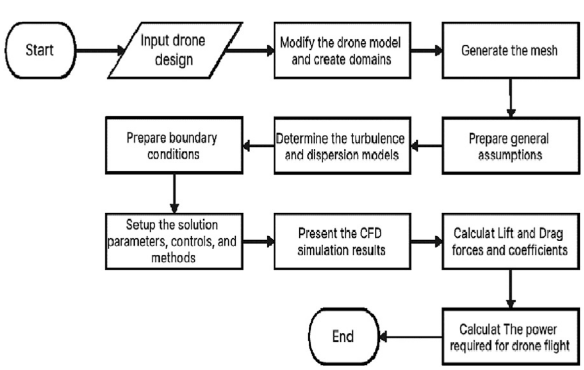

Fig. 6. The wind tunnel experience simulation methodology.

3. Results and discussions

Fig. 9 shows the spatial distribution of ScanEagle drone launch ban hours when weather systems in Iraq are present at the surface level. Launch prohibition was measured using data for five drone launch parameters due to climatic elements, temperature (T_max and T_min), precipitation, wind speed, and visibility for case studies of weather systems. It was noted that the Red Sea depression had the greatest impact on the launch of the drone, as it was attended to launch the ScanEagle 19–24 h a day, covering the largest area of Iraq, especially in the northern and eastern region, due to the heavy rains accompanying the Red Sea depression. The highest ScanEagle ban hours are concentrated in the northern region with the Mid-latitude depression, especially for class 19–24 h a day, and decrease as we head south. The southwestern region recorded the highest ScanEagle launch ban hours with the presence of Siberian high, reaching 18 h a day and

Table 3. Drone flight scenarios input to CFD analysis simulating wind tunnel experiment with UAV at surface layer.

Scenarios	Weather system	Station	Time	Wind speed (m/s)	Temperature (°K)	Pressure (Pa)	Density (kg/m^3)
1	Mid latitude	Erbil	2023-02-07 14:00:00	4.7	282	96,315	1.19
2	Mid latitude	Baghdad	2023-02-07 14:00:00	3.9	290	100,708	1.21
3	Mid latitude	Rutbah	2023-02-07 14:00:00	10.2	283	93,181	1.15
4	Mid latitude	Basrah	2023-02-07 14:00:00	5.2	292	100,810	1.20
5	Red Sea	Erbil	2023-03-26 14:00:00	3.7	288	96,276	1.16
6	Red Sea	Baghdad	2023-03-26 14:00:00	8.4	292	100,146	1.19
7	Red Sea	Rutbah	2023-03-26 14:00:00	7.8	288	92,787	1.12
8	Red Sea	Basrah	2023-03-26 14:00:00	11.1	294	100,294	1.19
9	Subtropical	Erbil	2023-04-14 14:00:00	2.4	291	97,474	1.20
10	Subtropical	Baghdad	2023-04-14 14:00:00	1.7	296	101,577	1.23
11	Subtropical	Rutbah	2023-04-14 14:00:00	2.2	293	94,182	1.16
12	Subtropical	Basrah	2023-04-14 14:00:00	3.3	300	101,393	1.22
13	Monsoon	Erbil	2023-07-24 14:00:00	4.8	318	94,973	1.04
14	Monsoon	Baghdad	2023-07-24 14:00:00	3.9	319	98,972	1.08
15	Monsoon	Rutbah	2023-07-24 14:00:00	6.1	313	92,384	1.03
16	Monsoon	Basrah	2023-07-24 14:00:00	6.3	319	98,982	1.08
17	Siberian	Erbil	2023-12-27 14:00:00	2.3	285	97,627	1.19
18	Siberian	Baghdad	2023-12-27 14:00:00	1.5	290	101,832	1.22
19	Siberian	Rutbah	2023-12-27 14:00:00	4.9	286	94,324	1.15
20	Siberian	Basrah	2023-12-27 14:00:00	2.6	295	101,682	1.20
21	Mid latitude	Erbil	2023-02-07 02:00:00	3.6	283	96,247	1.18
22	Mid latitude	Baghdad	2023-02-07 02:00:00	3.8	286	100,660	1.23
23	Mid latitude	Rutbah	2023-02-07 02:00:00	8.4	279	93,151	1.16
24	Mid latitude	Basrah	2023-02-07 02:00:00	1.9	284	100,694	1.23
25	Red Sea	Erbil	2023-03-26 02:00:00	3.2	290	96,333	1.16
26	Red Sea	Baghdad	2023-03-26 02:00:00	4.5	293	100,223	1.19
27	Red Sea	Rutbah	2023-03-26 02:00:00	2.4	287	92,694	1.13
28	Red Sea	Basrah	2023-03-26 02:00:00	5.0	294	100,435	1.19
29	Subtropical	Erbil	2023-04-14 02:00:00	2.5	284	97,221	1.23
30	Subtropical	Baghdad	2023-04-14 02:00:00	2.0	287	101,460	1.27
31	Subtropical	Rutbah	2023-04-14 02:00:00	3.8	281	94,090	1.20
32	Subtropical	Basrah	2023-04-14 02:00:00	2.4	288	101,442	1.27
33	Monsoon	Erbil	2023-07-24 02:00:00	0.9	303	95,271	1.10
34	Monsoon	Baghdad	2023-07-24 02:00:00	3.8	305	99,284	1.14
35	Monsoon	Rutbah	2023-07-24 02:00:00	5.1	298	92,735	1.08
36	Monsoon	Basrah	2023-07-24 02:00:00	4.6	304	99,234	1.14
37	Siberian	Erbil	2023-12-27 02:00:00	1.6	279	97,884	1.22
38	Siberian	Baghdad	2023-12-27 02:00:00	3.0	283	102,073	1.26
39	Siberian	Rutbah	2023-12-27 02:00:00	3.4	280	94,581	1.18
40	Siberian	Basrah	2023-12-27 02:00:00	3.4	284	101,894	1.25

decreasing as we headed north and east. No danger was recorded when launching the drone in the presence of Subtropical high and Monsoon low.

Fig. 10 shows the spatial distribution of ScanEagle flight ban hours in the presence of weather systems in Iraq at the 700 hPa level. The flight ban was measured using four drone flight limitation parameters due to climatic elements: temperature (T_max and T_min), wind speed, and relative humidity for case studies of weather systems. The highest no-fly hours for ScanEagle were in the presence of the Mid-latitude depression, which covered the largest area of Iraq, in the northern, western, and southern regions, ranging from 19 to 24 h a day. The no-fly hours, with the presence of Red Sea depression, Monsoon low, Siberian high, and Subtropical high, were few and concentrated in the southern region and decreased as we headed north. The class from 0 to 6 h per day dominates most of the area of Iraq.

Fig. 11 shows the change in aerodynamic forces (lift and drag) for ScanEagle flight in the surface weather scenarios at 02:00 and 14:00. In general, there is a direct proportion between drag and lift, i.e., when drag increases due to an increase in headwind speed, for example, the lift will also increase for the same reason. This can maintain the stability of the drone, but it requires greater thrust to overcome the increase in additional drag to maintain a constant flight speed. Additional thrust can be generated by increasing engine power through increased fuel burn, which reduces

Table 4. Drone flight scenarios input to CFD analysis simulating wind tunnel experiment with UAV at 700 hPa.

Scenarios	Weather system	Station	Time	Wind speed (m/s)	Temperature (°K)	Density (kg/m^3)
41	Mid latitude	Erbil	2023-02-07 14:00:00	14.5	263	0.96
42	Mid latitude	Baghdad	2023-02-07 14:00:00	13.3	265	0.95
43	Mid latitude	Rutbah	2023-02-07 14:00:00	23.0	263	0.96
44	Mid latitude	Basrah	2023-02-07 14:00:00	19.0	272	0.92
45	Red Sea	Erbil	2023-03-26 14:00:00	7.0	272	0.92
46	Red Sea	Baghdad	2023-03-26 14:00:00	6.9	273	0.92
47	Red Sea	Rutbah	2023-03-26 14:00:00	9.4	272	0.93
48	Red Sea	Basrah	2023-03-26 14:00:00	10.5	275	0.92
49	Subtropical	Erbil	2023-04-14 14:00:00	6.0	269	0.94
50	Subtropical	Baghdad	2023-04-14 14:00:00	8.4	273	0.92
51	Subtropical	Rutbah	2023-04-14 14:00:00	7.8	275	0.92
52	Subtropical	Basrah	2023-04-14 14:00:00	11.9	277	0.91
53	Monsoon	Erbil	2023-07-24 14:00:00	4.7	290	0.87
54	Monsoon	Baghdad	2023-07-24 14:00:00	3.7	287	0.88
55	Monsoon	Rutbah	2023-07-24 14:00:00	8.1	287	0.88
56	Monsoon	Basrah	2023-07-24 14:00:00	9.2	288	0.87
57	Siberian	Erbil	2023-12-27 14:00:00	6.3	273	0.92
58	Siberian	Baghdad	2023-12-27 14:00:00	6.0	274	0.92
59	Siberian	Rutbah	2023-12-27 14:00:00	5.9	274	0.92
60	Siberian	Basrah	2023-12-27 14:00:00	6.6	276	0.91
61	Mid latitude	Erbil	2023-02-07 02:00:00	14.8	264	0.95
62	Mid latitude	Baghdad	2023-02-07 02:00:00	18.0	265	0.95
63	Mid latitude	Rutbah	2023-02-07 02:00:00	22.3	264	0.95
64	Mid latitude	Basrah	2023-02-07 02:00:00	22.4	271	0.93
65	Red Sea	Erbil	2023-03-26 02:00:00	9.8	273	0.92
66	Red Sea	Baghdad	2023-03-26 02:00:00	17.5	273	0.92
67	Red Sea	Rutbah	2023-03-26 02:00:00	3.5	272	0.93
68	Red Sea	Basrah	2023-03-26 02:00:00	14.8	274	0.92
69	Subtropical	Erbil	2023-04-14 02:00:00	6.8	267	0.94
70	Subtropical	Baghdad	2023-04-14 02:00:00	11.7	269	0.93
71	Subtropical	Rutbah	2023-04-14 02:00:00	10.1	271	0.93
72	Subtropical	Basrah	2023-04-14 02:00:00	20.3	270	0.93
73	Monsoon	Erbil	2023-07-24 02:00:00	3.5	290	0.87
74	Monsoon	Baghdad	2023-07-24 02:00:00	5.1	288	0.87
75	Monsoon	Rutbah	2023-07-24 02:00:00	10.6	287	0.88
76	Monsoon	Basrah	2023-07-24 02:00:00	3.1	289	0.87
77	Siberian	Erbil	2023-12-27 02:00:00	6.1	275	0.92
78	Siberian	Baghdad	2023-12-27 02:00:00	5.7	275	0.92
79	Siberian	Rutbah	2023-12-27 02:00:00	8.5	275	0.92
80	Siberian	Basrah	2023-12-27 02:00:00	13.5	276	0.91

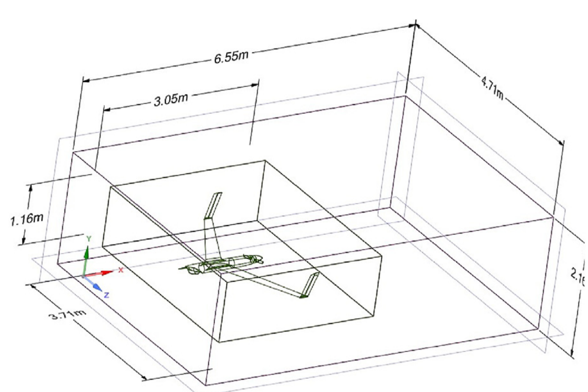

Fig. 7. Wind tunnel domains dimensions.

Table 5. ScanEagle geometry modification results.

Object Name	Inner domain	Outer domain
Volume	13.12598 m^3	66.63708 m^3
Nodes	2,657,393	455,459
Elements	15,397,032	426,199
Method	Tetrahedrons	Hex Dominant
Max_Element size	2.e-002 m	5.e-002 m
Smoothing	High	
Mesh Metric Aspect ratio (average)	1.77991684617	1.02831163963
Mesh Metric element Quality (average)	0.85441494274	0.996875710855
Mesh Metric Skewness (average)	0.201882003783	0.012164890820
Orthogonal Quality (average)	0.797015510917	0.997817037476

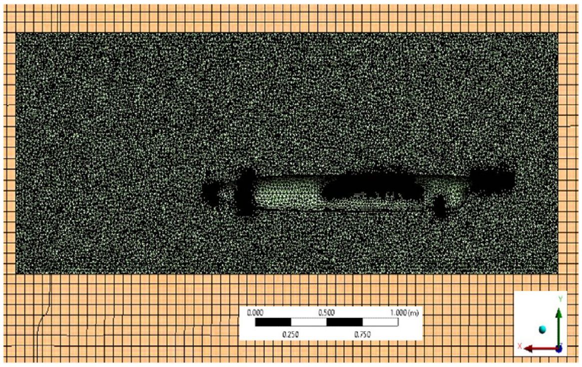

Fig. 8. The mesh method and shape.

endurance (the longest possible flight time). The drag and lift forces at 14:00 are greater than at 02:00 due to increased instability resulting from the increase in temperature and wind speed.

The highest values of lift and drag forces were in the presence of Red Sea depression and Mid-latitude depression compared to other weather systems as shown in Fig. 11 (A) and (B), respectively, as they were the highest in Basra and Baghdad stations with Red Sea depression and in Rutba and Erbil stations with Mid-latitude depression, because the effect of the first system is greater in the southern and central region and the effect of the

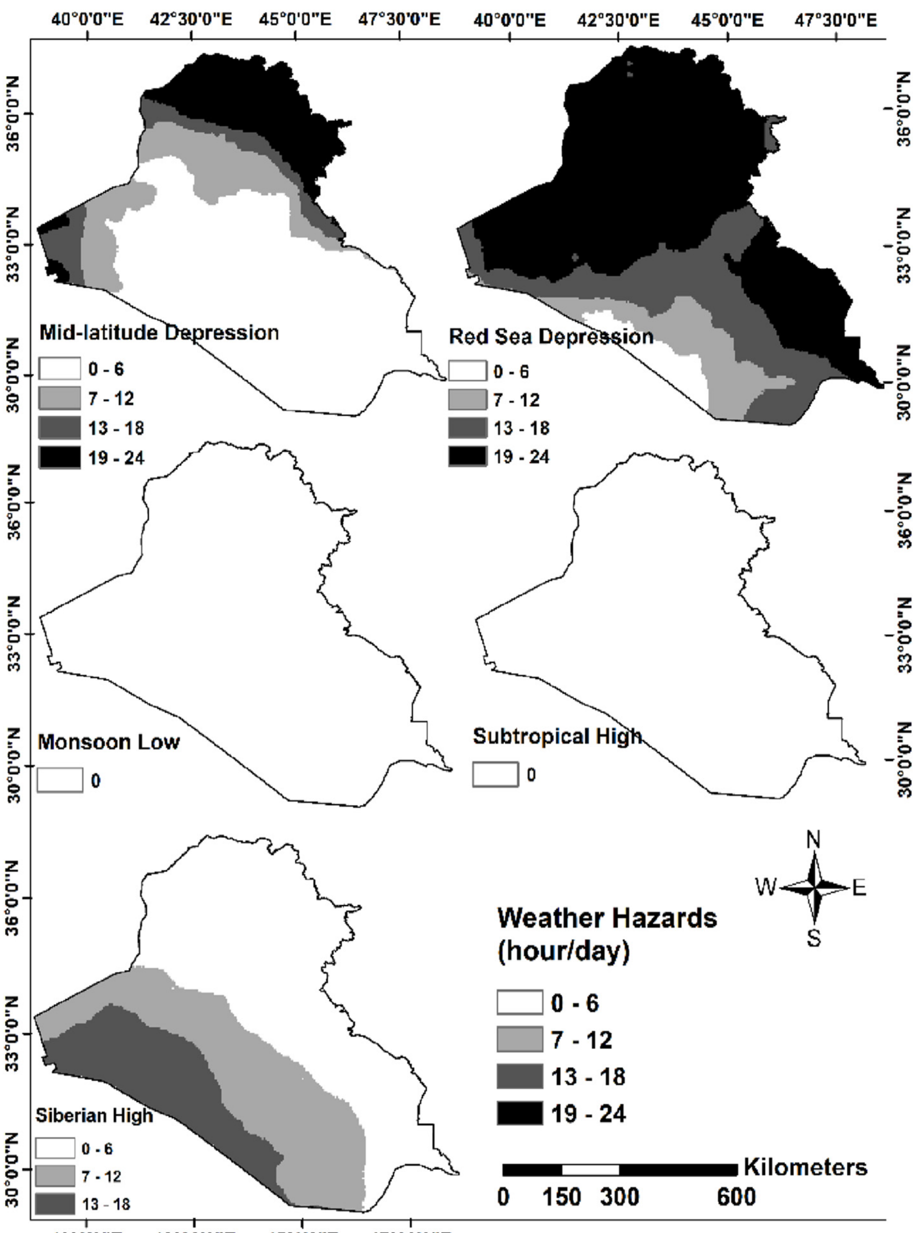

Fig. 9. Launch ban hours of due to weather hazards at the surface level.

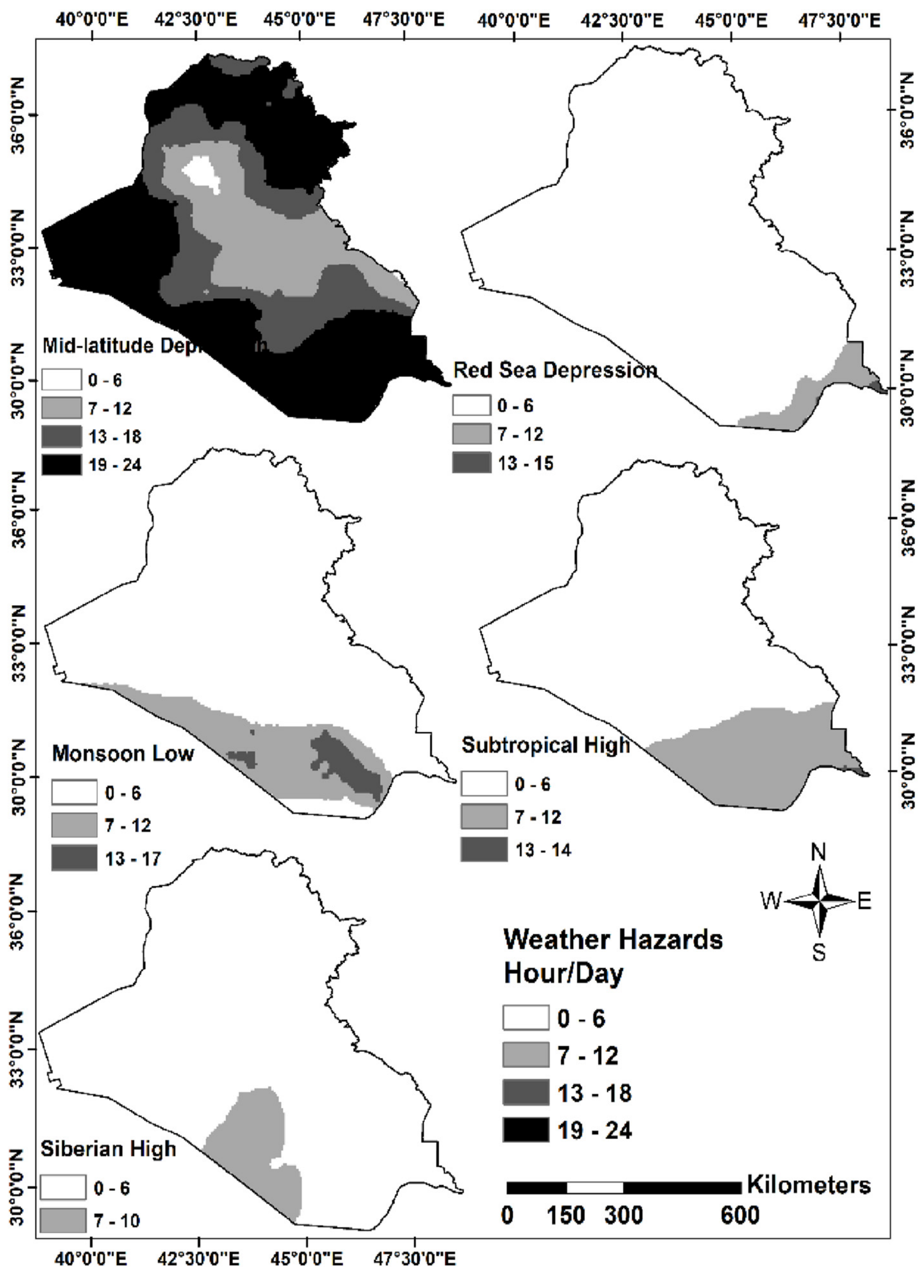

Fig. 10. Flight ban hours due to weather hazards at the 700 hPa level.

second system is greater in the northern and western region due to the path of the system. The forces are relatively less in the presence of Monsoon low and Siberian high and greater than Subtropical high, as in Fig. 11 (C), (E), and (D), respectively.

Fig. 12 shows the average lift and drag forces at the four ScanEagle flight stations in the weather system scenarios at 02:00 and 14:00. The highest values of the forces are with the red Sea depression, then the Mid latitude depression, and the Monsoon low, respectively. The values are lowest with the Siberian high and the Subtropical high. The forces at 02:00 are higher than at 14:00 with the two highs.

Fig. 13 shows the Power Required (PR) for ScanEagle flying at constant speed (25 m/s) at 02:00 and 14:00 for scenarios in the surface layer of weather systems. Power required is directly proportional to drag and wind speed. At 14:00 PR is highest with Red Sea depression, then Mid-latitude depression, Monsoon low, Siberian high, and Subtropical high are lowest, respectively. At 02:00 PR is highest with Mid latitude depression and Red Sea depression. The value is close to Siberian high, Subtropical high, and Monsoon low.

Fig. 14 shows the change in aerodynamic coefficients (lift and drag) for ScanEagle flight in

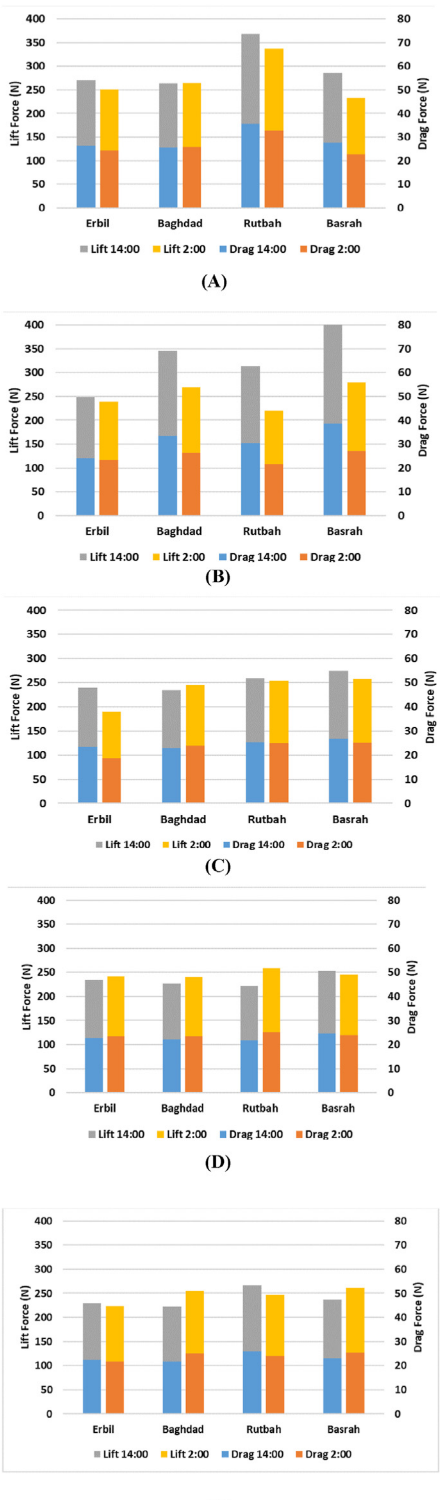

Fig. 11. *Lift and drag forces from the ScanEagle wind tunnel flight experiment in the weather system scenarios at the surface at 02:00 and 14:00. (A) Mid-latitude depression, (B) Red Sea depression, (C) Monsoon low, (D) Siberian high, and (E) Subtropical high.*

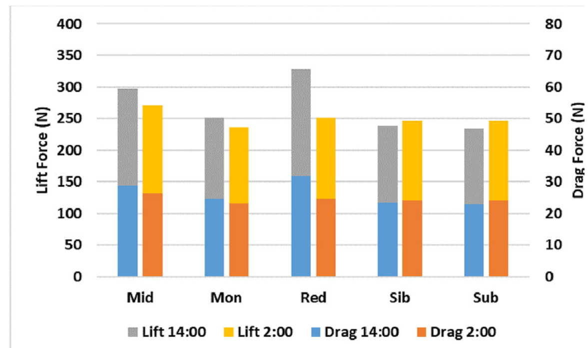

Fig. 12. *Average lift and drag forces in the surface layer for weather system scenarios at 02:00 and 14:00.*

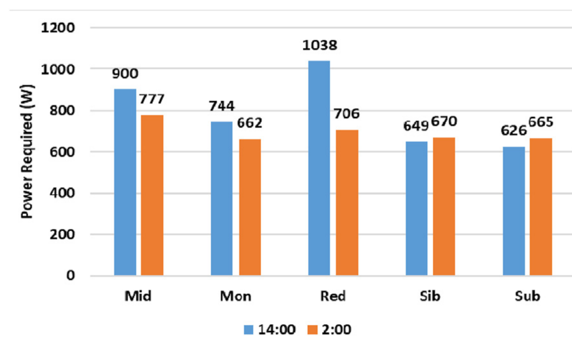

Fig. 13. *The power required at constant speed (25 m/s) at 02:00 and 14:00 for scenarios in the surface layer.*

weather system scenarios at 700 hPa at 02:00 and 14:00. In general, there is a direct proportion between drag and lift. The drag and lift forces at 14:00 are greater than those at 02:00 due to the increase in instability resulting from the increase in temperature and wind speed. The highest values of lift and drag forces were with the presence of Mid-latitude depression at all stations, especially Basra and Rutba stations, with a large difference from the rest of the weather systems due to the high wind speed accompanying the depression. The values of lift and drag forces vary between stations in the Red Sea depression, Siberian high, and Subtropical high due to the fluctuation of wind speed at the 700 hPa level. The values were the lowest with Monsoon.

Fig. 15 shows the lift and drag forces at 700 hPa for ScanEagle flight at four stations in the weather system scenarios at 02:00 and 14:00. Mid latitude depression has the greatest influence on drone flight compared to other weather systems. It is followed by Subtropical high, then Red Sea depression, and Siberian high, and the weather system with the least influence is Monsoon low.

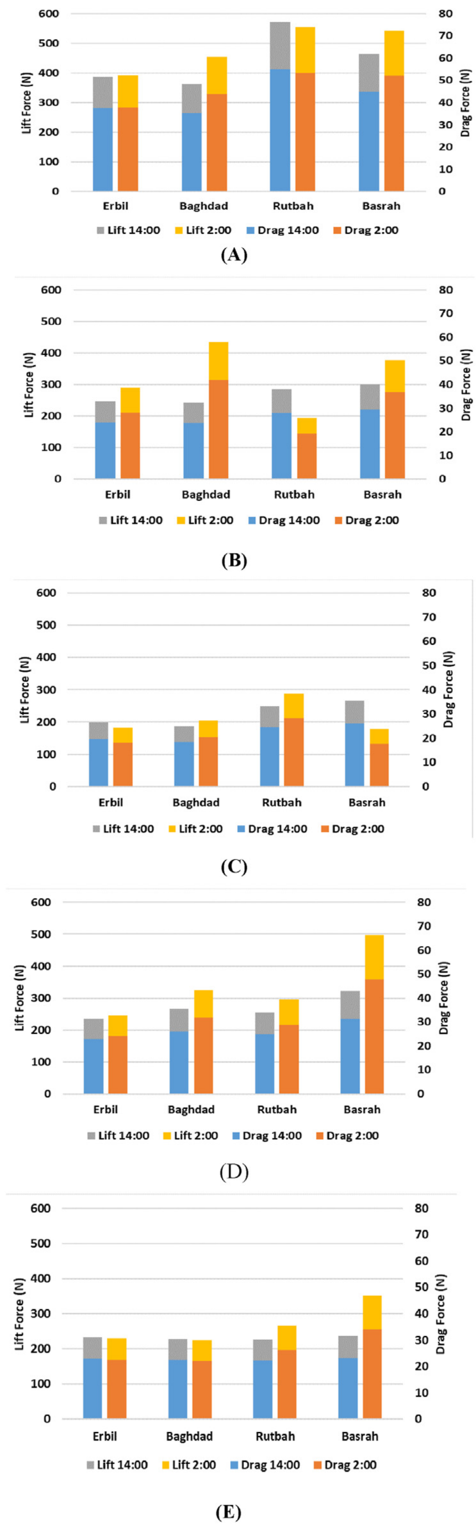

Fig. 14. Lift and drag forces for ScanEagle flight at 700 hPa scenarios at 02:00 and 14:00. (A) Mid-latitude depression, (B) Red Sea depression, (C) Monsoon low, (D) Siberian high, and (E) Subtropical high.

Fig. 16 shows the power required for a ScanEagle to fly at a constant speed (25 m/s) at 02:00 and 14:00 for the 700 hPa weather system scenarios. Generally, the PR at 700 hPa is much higher than that required

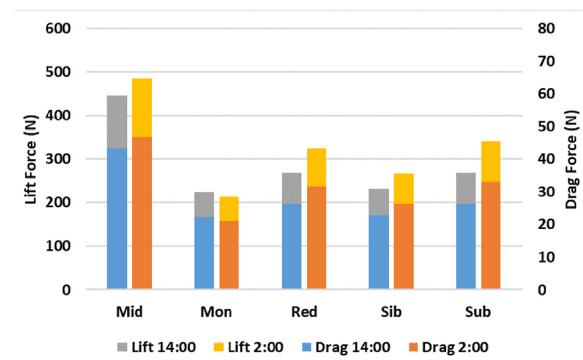

Fig. 15. Lift and drag ratios at 700 hPa for weather system scenarios at 02:00 and 14:00.

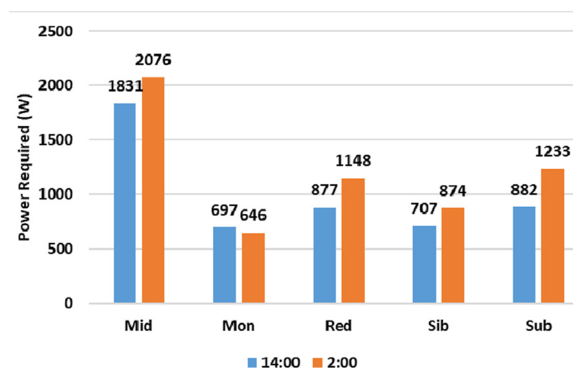

Fig. 16. The Power required at constant speed (25 m/s) at 02:00 and 14:00 for scenarios 700 hPa.

at the surface because the wind speed at this level is higher than at the surface. It is observed that the Mid latitude depression has the greatest effect on the PR and thus has the greatest effect on the fuel consumption of the drone to maintain a constant flight speed. It is followed by the Subtropical high, then the Red Sea depression, and the Siberian high, and the weather system with the least effect is the Monsoon low.

4. Conclusions

ScanEagle drones should be banned in Iraq in the presence of the Red Sea depression because the 24-h drone no-fly zone at surface covers most of its area. It should be banned in the northern region in the presence of mid-latitude depressions, and they should fly at low levels in the rest of the regions in case we need to use them because the drone no-fly zone at 700 hPa for 24 h covers most of its area. The greatest impact on drone flight in Iraq was with the presence of Red Sea depressions and mid-latitude depressions, as the aerodynamic forces (lift and drag) increased and thus the power required for constant speed flight increased, which increased fuel consumption and flight time. It reached 1038 w at the surface with the Red Sea depression and 2076 W at 700 hPa with the mid-latitude depression, which is more than three times the power required to operate the drone in the Monsoon low. The effect of Red Sea depression is greatest in the central and southern regions, but mid-latitude depressions have the greatest impact on the northern and western regions and affect the entire area of Iraq in the case of flying at the 700 hPa level. The aerodynamic forces of the drone increase as the flight level increases due to the decrease in pressure and density and the increase in wind speed, so the power required to maintain its speed increases. For example, the required power was 1038 W at the surface with a mid-latitude depression at night, and it was 2076 W at 700 hPa, which was double the required power. Which reduces the flight time (endurance) due to the increase in fuel burn or battery consumption for drones that depend on it as a source of energy.

Ethics information

All research activities complied with relevant ethical standards for studies without human or animal subjects.

Funding

The authors did not receive support from any organization for the submitted work.

Acknowledgment

The authors would like to thank Mustansiriya University, Baghdad, Iraq, for their cooperation in realizing the present work.

References

[1] A.S. Saeed, A.B. Younes, C. Cai, G. Cai, A survey of hybrid unmanned aerial vehicles, Prog. Aero. Sci. 98 (2018) 91−105, https://doi.org/10.1016/j.paerosci.2018.03.007.
[2] F. Costache, S.E. Nichifor, M.L. Costea, A. Ionita, Automatic approach procedure of a flying vehicle on a mobile platform using backstepping controller, INCAS Bulletin 14 (2022) 51−62, https://doi.org/10.13111/2066-8201.2022.14.4.5.
[3] A. Otto, N. Agatz, J. Campbell, B. Golden, E. Pesch, Optimization approaches for civil applications of unmanned aerial vehicles (UAVs) or aerial drones: a survey, Networks 72 (2018) 411−458, https://doi.org/10.1002/net.21818.
[4] Y. Averyanova, E. Znakovskaja, Weather hazards analysis for small UAVs durability enhancement, in: IEEE 6th International Conference on Actual Problems of Unmanned Aerial Vehicles Development (APUAVD), IEEE Xplore, Kyiv, Ukraine. (2021), pp. 41−44.
[5] M. Gao, C.H. Hugenholtz, T.A. Fox, M. Kucharczyk, T.E. Barchyn, P.R. Nesbit, Weather constraints on global drone flyability, Sci. Rep. 11 (2021) 12092, https://doi.org/10.1038/s41598-021-91325-w.
[6] K. Telli, O. Kraa, Y. Himeur, A. Ouamane, M. Boumehraz, S. Atalla, W. Mansoor, A Comprehensive review of recent research trends on Unmanned Aerial Vehicles (UAVs), Systems 11 (2023) 400, https://doi.org/10.3390/systems11080400.
[7] A.H. Al-Muhyi, F.Y. Aleedani, M.Q. Albattat, J.M. Badr, Rainfall Repercussions: assessing climate change influence on Iraq precipitation patterns, Al-Kitab J. Pure Sci. 8 (2024) 92−103, https://doi.org/10.32441/kjps.08.01.p9.
[8] Y.A. Shaghati, Study of some patterns for severe rainfalls over Iraq, Al-Mustansiriyah J. Sci. 31 (2020) 9−14, https://doi.org/10.23851/mjs.v31i4.878.
[9] H. Babaousmail, R. Hou, B. Ayugi, M. Ojara, H. Ngoma, R. Karim, A. Rajasekar, V. Ongoma, Evaluation of the performance of CMIP6 models in reproducing rainfall patterns over north Africa, Atmosphere 12 (2021) 475, https://doi.org/10.3390/atmos12040475.
[10] L. Lee, B. Pang, Kin Huat Low, Environmental data analytics for safe drone operations in low-altitude urban environments, in: AIAA AVIATION 2022 Forum, 2022, p. 3405, https://doi.org/10.2514/6.2022-3405.
[11] A. Allouch, A. Koubâa, M. Khalgui, T. Abbes, Qualitative and quantitative risk analysis and safety assessment of unmanned aerial vehicles missions over the internet 7, IEEE Access. (2019), pp. 53392−53410, https://doi.org/10.1109/ACCESS.2019.2911980.
[12] A. Bajaj, B. Philips, E. Lyons, D. Westbrook, M. Zink, Determining and communicating weather risk in the new drone economy, in: 2020 IEEE 92nd Vehicular Technology Conference (VTC2020-Fall), Victoria, BC, Canada, 2020, pp. 1−6, https://doi.org/10.1109/vtc2020-fall49728.2020.9348845.
[13] M. Gianfelice, H. Aboshosha, T. Ghazal, Real-time wind predictions for safe drone flights in Toronto, Results Eng. 15 (2022) 100534, https://doi.org/10.1016/j.rineng.2022.100534.
[14] P.-C. Shao, Risk assessment for UAS logistic delivery under UAS traffic management environment, Aerospace 7 (2020) 140, https://doi.org/10.3390/aerospace7100140.
[15] N. Raballand, S. Bertrand, S. Lala, B. Levasseur, DROSERA: a DROne simulation environment for risk assessment, in: Proceedings of the 31st European Safety and Reliability Conference (ESREL 2021), 2021, pp. 354−361, https://doi.org/10.3850/978-981-18-2016-8_236-cd.
[16] S. Kocsis Szürke, N. Perness, P. Földesi, D. Kurhan, M. Sysyn, S. Fischer, A risk assessment technique for energy efficient drones to support pilots and ensure safe flying, Infrastructures 8 (2023) 67, https://doi.org/10.3390/infrastructures8040067.
[17] G. Radzki, P. Golinska-Dawson, G. Bocewicz, Z. Banaszak, Modelling robust delivery scenarios for a fleet of unmanned aerial vehicles in disaster relief missions, J. Intell. Rob. Syst. 103 (2021) 63, https://doi.org/10.1007/s10846-021-01502-2.
[18] O.F. Khayoon, O.T. Al-Taai, Severe meteorological factors affecting civil aviation flights at Iraqi airports, Al-Mustansiriyah J. Sci. 33 (2022) 15−26, https://doi.org/10.23851/mjs.v33i4.1179.
[19] H.Q. Adeeb, Y.K. Al-Timimi, GIS techniques for mapping of wind speed over Iraq, Iraqi J. Agric. Sci. 50 (2019) 1621−1629, https://doi.org/10.36103/ijas.v50i6.852.
[20] S. Aljuhaishi, Y. Al-Timimi, B. Wahab, Weather constraints on drone flyability in Iraq, Papers Appl. Geogr. 10 (2024) 1−15, https://doi.org/10.1080/23754931.2024.2400280.
[21] L. Zangana, B.W. Al-Temimi, S. Aljuhaishi, Analytical study of rate volume liquid water content in low clouds over Iraq, Iraqi J. Agric. Sci. 52 (2021) 783−792, https://doi.org/10.36103/ijas.v52i4.1387.
[22] Y.K. Al-Timimi, A.A. Al-Khudhairy, Spatial and temporal temperature trends on Iraq during 1980-2015, J. Phys. Conf. 1003 (2018) 012091, https://doi.org/10.1088/1742-6596/1003/1/012091.
[23] A.-Z.A. Mohsen, M.H. Al-Jiboori, Y.K. Al-Timimi, Investigating the aerodynamic surface roughness length over Baghdad city utilizing remote sensing and GIS techniques,

Baghdad Sci. J. 18 (2021) 1048, https://doi.org/10.21123/bsj.2021.18.2(suppl.).1048.
[24] M.A. Al-Obaidi, Y.K. AL-Timimi, Change detection in Mosul dam lake, north of Iraq using remote sensing and GIS techniques, Iraqi J. Agric. Sci. 53 (2022) 38–47, https://doi.org/10.36103/ijas.v53i1.1506.
[25] Y.K. Al-Timimi, Monitoring desertification in some regions of Iraq using GIS Techniques, Iraqi J. Agric. Sci. 52 (2021) 620–625, https://doi.org/10.36103/ijas.v52i3.1351.
[26] S.Q. Al-Jbouri, Y.K. Al-Timimi, Assessment of relationship between land surface temperature and normalized different vegetation index using Landsat images in some regions of Diyala governorate, Iraqi J. Agric. Sci. 52 (2021) 793–801, https://doi.org/10.36103/ijas.v52i4.1388.
[27] Y.K. Al-Timimi, A.M. Al-Lami, H.K.A. Al-Shamarti, S.K. Al-Maamory, Analysis of some extreme temperature indices over Iraq, Mausam 71 (2021) 423–430, https://doi.org/10.54302/mausam.v71i3.40.
[28] S.H. Halos, S. Mahdi, Effect of climate change on spring massive sand/dust storms in Iraq, Al-Mustansiriyah J. Sci. 32 (2021) 13–20, https://doi.org/10.23851/mjs.v32i4.1105.
[29] Daily climate composites: NOAA physical sciences laboratory. Psl.noaa.gov, 2022. (accessed October 18 2022). https://psl.noaa.gov/data/composites/day/.
[30] R.F. Edwing, NOAA's Physical oceanographic real time system (PORTS®), J. Oper. Oceanogr. 12 (2018) S176–S186, https://doi.org/10.1080/1755876x.2018.1545558.
[31] H. Setchell, ECMWF reanalysis v5, ECMWF. https://www.ecmwf.int/en/forecasts/dataset/ecmwf-reanalysis-v5, 2020. (accessed October 18 2022).
[32] J. Mohammed Ali, S.K. Mohammed, J.H. Kadhum, Climate index; cold events; extreme; precipitations, Al-Mustansiriyah J. Sci. 32 (2021) 63, https://doi.org/10.23851/mjs.v32i2.985.
[33] H.W. Chen, L.N. Zhang, F. Zhang, K.J. Davis, T. Lauvaux, S. Pal, B. Gaudet, J.P. DiGangi, Evaluation of regional CO_2 mole fractions in the ECMWF CAMS real-time atmospheric analysis and NOAA carbon tracker near real time reanalysis with airborne observations from ACT America field campaigns, J Geophys. Res. Atmos. 124 (2019) 8119–8133, https://doi.org/10.1029/2018jd029992.
[34] H. Flentje, I. Mattis, Z. Kipling, S. Rémy, W. Thomas, Evaluation of ECMWF IFSAER (CAMS) operational forecasts during cycle 41r1–46r1 with calibrated ceilometer profiles over Germany, Geosci. Model Dev. (GMD) 14 (2021) 1721–1751, https://doi.org/10.5194/gmd-14-1721-2021.
[35] A. Gore, B. Hale, P. Mcclure, Exploring Detection of Unmanned Aerial Systems on 5g Networks via Machine Learning, Thesis, Naval Postgraduate School Monterey, California. (2023). https://apps.dtic.mil/sti/trecms/pdf/AD1213284.pdf. (accessed September 9 2024).
[36] G. Zuliani, The next horizon: the future of unmanned aircraft systems in the Canadian armed forces, Canadian forces college, Canada. https://www.cfc.forces.gc.ca/259/290/308/305/zuliani.pdf, 2019. (accessed September 9 2024).
[37] T.J. Zajkowski, M.B. Dickinson, J.K. Hiers, W. Holley, B.W. Williams, A. Paxton, O. Martinez, G.W. Walker, Evaluation and use of remotely piloted aircraft systems for operations and research - RxCADRE 2012, Int. J. Wildland Fire 25 (2016) 114–128, https://doi.org/10.1071/wf14176.
[38] A. Hodgson, D. Peel, N. Kelly, Unmanned aerial vehicles for surveying marine fauna: assessing detection probability, Ecol. Appl. 27 (2017) 1253–1267, https://doi.org/10.1002/eap.1519.
[39] E.E. Moreland, M.F. Cameron, R.P. Angliss, P.L. Boveng, Evaluation of a ship-based unoccupied aircraft system (UAS) for surveys of spotted and ribbon seals in the Bering Sea pack ice, J. Unmanned Veh. Syst. 3 (2015) 114–122, https://doi.org/10.1139/juvs-2015-0012.
[40] A. Hodgson, N. Kelly, D. Peel, Unmanned Aerial Vehicles (UAVs) for surveying marine fauna: a Dugong case study, PLoS One 8 (2013) e79556, https://doi.org/10.1371/journal.pone.0079556.
[41] S. Aljuhaishi, Y.K. Al-Timimi, B.I. Wahab, Comparing turbulence models for CFD simulation of UAV flight in a wind tunnel experiments, Period. Polytech. Transp. Eng. 52 (2024) 301–309, https://doi.org/10.3311/pptr.24004.